Available online at www.sciencedirect.com
ScienceDirect
Construction and Building Materials 22 (2008) 1129–1136
Construction and Building MATERIALS
www.elsevier.com/locate/conbuildmat

Numerical analysis of localized steel corrosion in concrete

Chin-Yong Kim *, Jin-Keun Kim

Department of Civil and Environmental Engineering, Korea Advanced Institute of Science and Technology (KAIST), 373-1, Guseong-dong, Yuseong-gu, Daejeon, 305-701, Republic of Korea

Received 24 January 2007; received in revised form 26 February 2007; accepted 27 February 2007
Available online 12 April 2007

Abstract

Although the existing studies on the estimation of corrosion induced cracking time of concrete cover practically assumed that the shape of corrosion product is uniform, experimental observations show that the shape of the corrosion product is considerably localized. In this study, numerical estimation of localized corrosion was accomplished based on the assumption that the main cause of corrosion localization is the variation of chloride ions around the steel. The target case was limited to a two-dimensional corrosion. Analysis results show that the maximum corrosion depth remains about 1.3 ~ 3.5 times deeper than the average corrosion depth after 3.5 years of active corrosion. Parametric study reveals that the diffusion coefficient of chloride ion is the parameter most responsible for corrosion localization.

Keywords: Chloride ion; Corrosion

1. Introduction

Chloride ion induced corrosion of steel is one of the most important causes of deterioration in reinforced concrete (RC) structures. Generally, the chloride ion induced deterioration process can be divided into two stages: (1) initiation stage – period from the placement of RC structures to the initiation of steel corrosion in concrete; and (2) propagation stage – period from the onset of steel corrosion to the moment when RC structures lose their serviceability in the form of cracking, spalling of concrete cover, etc. For the propagation stage, the cracking time of concrete cover is recognized as a primary concern and much effort has been devoted to study of this aspect [1–8]. In these studies, the shape of corrosion products are usually assumed to be uniform, that is, the radial expansion of steel due to corrosion is the same for all directions. In a real case, however, the distribution of corrosion products is highly localized; usually, more corrosion product is accumulated where the concentration of chloride ions is higher [8,9].

Owing to recent numerical studies on steel corrosion in concrete, it is well documented that the fundamental theories of electrochemistry can be successfully applied to RC structures for the evaluation of steel corrosion [7,10–15]. While research to date has yielded valuable insights, the circumferential variation of corrosion behavior along the steel surface has not been considered. Steel has been treated as an ideal line element with a zero cross sectional area. Although this assumption might be sufficient for the analysis of large scale macro-cell corrosion in which the anodic and cathodic regions of steel are clearly separated longitudinally, it is not suitable for the analysis of general corrosion in which the variation of chloride ions around the steel may cause small scale macro-cell corrosion between the upper and the lower portion of the steel surface. Notably, it is clear from experimental and analytical evidence, that the concentration of chloride ions can vary considerably around the steel surface, because of the impermeable nature of steel [9,16,17]; more chloride ions are accumulated on the steel surface facing the exposed surface of concrete. According to the theory

* Corresponding author. Tel.: +82 42 869 3654; fax: +82 42 869 3688.
E-mail address: chinyong0@kaist.ac.kr (C.-Y. Kim).

0950-0618/$ - see front matter © 2007 Elsevier Ltd. All rights reserved.
doi:10.1016/j.conbuildmat.2007.02.007

of electrochemistry, this phenomenon can cause highly concentrated corrosion at chloride ion rich areas, as illustrated in Fig. 1. It is clear that the localized corrosion products would accelerate the rate of crack propagation in the concrete cover. For the same corrosion rate, the duration of propagation stage determined based on the uniform corrosion is much longer than that based on the localized corrosion. Consequently, unless the localized feature of corrosion is considered, the cracking time of concrete cover calculated from the analytical methods could considerably overestimate that of RC structures exposed to the natural environment for a given value of corrosion rate.

The main goal of this research work is to provide a reasonable estimation of localized corrosion, which can be in turn used for a more precise assessment of cracking time. It was assumed that the main cause of localized corrosion is the variation of chloride ions around the steel surface. The target cases were limited to the two-dimensional corrosion in which the variation of chloride ions and oxygen along the longitudinal direction of steel can be neglected. A parametric study was also performed to investigate the influence of some material parameters on the rate and localization of corrosion.

2. Models for the corrosion analysis

2.1. Penetration of chloride ions and oxygen

In the present work, the penetration of chloride ions and oxygen is considered as a pure diffusion process, as the main concern of this paper is a corrosion analysis considering the concentration variation around the steel, not an exact description of the concentration profile of chloride ions or oxygen. Diffusion coefficients of chloride ion and oxygen are treated as user input values.

2.2. Steel corrosion

2.2.1. General

Corrosion of steel is composed of two electrode reactions: (1) anodic reaction – dissolution of iron to Fe^{2+} ions; and (2) cathodic reaction – reduction of oxygen to OH^- ions (in common environment). The difference in electric potential between the interior of the electrodes and the ions in the surrounding electrolyte is called the electrode potential. At equilibrium and an open circuit condition, the rate of oxidation (reaction losing electrons) and reduction (reaction getting electrons) at the electrode is the same. The electrode potential and the exchanging current density (proportional to the rate of oxidation or reduction) at equilibrium are called the equilibrium potential and the exchange current density, respectively. If over potential or net current is applied to electrodes, the equilibrium condition is disturbed; net current starts flowing or the equilibrium potential is altered at the electrodes. The extent of potential change caused by the net current at the electrodes, measured in volts, is called polarization. There are three causes of polarization: concentration, activation, and ohmic potential drop.

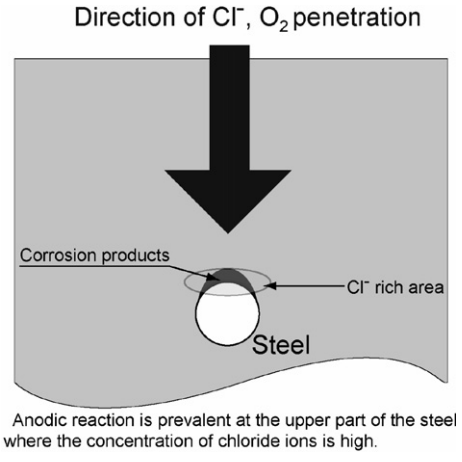

Fig. 1. Description of the localized corrosion.

2.2.2. Polarization of cathodes

If the amount of available oxygen is not sufficient for the cathodic reaction, the concentration polarization controls the polarization of cathodes. Concentration polarization at the cathodes, $\eta_{c,c}$ (V), can be calculated as [18]:

$$\eta_{c,c} = -\frac{RT}{zF}\ln\frac{i_L}{i_L - i_c} \tag{1}$$

where R is the universal gas constant (=8.314 J/K mol), T is the absolute temperature (K), F is Faraday's constant (= 9.65×10^4 C/mol), z is the number of electrons exchanged in the cathodic reaction (=4), i_c is the cathodic current density (A/cm^2) and i_L is the limiting current density of the cathodic reaction (A/cm^2). The limiting current density is usually calculated from the concentration of oxygen on the steel surface [11,18]. In the authors' opinion, however, the factor that restricts the rate of cathodic reaction in RC structures is the limited supply of oxygen through the concrete cover not the concentration of oxygen on the steel surface. It is noted that the latter can be a limiting factor when the supply of oxygen is sufficiently high. Therefore, the limiting current density is calculated from the maximum supply of oxygen obtained from the steady-state analysis of oxygen penetration,

$$i_L = zFJ_{O_2,\max} \tag{2}$$

where $J_{O_2,\max}$ is the maximum supply of oxygen to the steel surface (mol/(cm^2 s)).

According to the Butler–Volmer kinetics, the activation polarization of the cathodes, $\eta_{c,a}$, can be expressed using the Tafel equation [18],

$$\eta_{c,a} = -\beta_c \log\frac{i_c}{i_{c0}} \tag{3}$$

where β_c is the Tafel slope of the cathodic reaction (V/decade) and i_{c0} is the exchange current density of the cathodic reaction (A/cm^2). By adding Eqs. (1) and (3), the polarization of the cathodes, η_c, can be expressed as Eq. (4).

$$\eta_c = -\beta_c \log\frac{i_c}{i_{c0}} - \frac{RT}{zF}\ln\frac{i_L}{i_L - i_c} \quad (4)$$

2.2.3. Polarization of anodes

It is assumed that the activation is the only cause of the anodic polarization. Hence the polarization of the anodes, η_a, can be calculated by the following equation [18],

$$\eta_a = \beta_a \log\frac{i_a}{i_{a0}} \quad (5)$$

where β_a is the Tafel slope of the anodic reaction (V/decade), i_a is the anodic current density (A/cm^2) and i_{a0} is the exchange current density of the anodic reaction (A/cm^2). In this study, β_a is assumed to be 90.7 mV/decade for depassivated steel and infinity for passive steel, and β_c is assumed to be 176.3 mV/decade for both states of steel [15].

2.2.4. Electrode potential and corrosion current density

From the polarization, electrode potentials for the anodes and the cathodes can be expressed as the following equations,

$$\phi_a = \phi_{a0} + \eta_a = \phi_{a0} + \beta_a \log\frac{i_a}{i_{a0}} \quad \text{(for the anodes)} \quad (6)$$

$$\phi_c = \phi_{c0} + \eta_c = \phi_{c0} - \beta_c \log\frac{i_c}{i_{c0}} - \frac{RT}{zF}\ln\frac{i_L}{i_L - i_c} \quad \text{(for the cathodes)} \quad (7)$$

where ϕ_a, ϕ_c are the anodic and cathodic potentials (V), and ϕ_{a0}, ϕ_{c0} are the equilibrium potentials of the anodes and cathodes (V) under a certain environment. For simplicity of the corrosion analysis, it is assumed in this study that ϕ_{a0} and ϕ_{c0} remain constant throughout the corrosion process. In reality, however, these values are dependent on the pH, fugacity of oxygen, and the ionic activity of iron [11,18].

If the value of potential at a certain point on the steel surface, ϕ_s, is known, corrosion current densities for the anodic and cathodic reaction at that point can be calculated by substituting ϕ_s for ϕ_a and ϕ_c in Eqs. (6) and (7). While the anodic current density can be obtained explicitly from Eq. (6), iteration is needed to find the cathodic current density from Eq. (7) because the limiting current density results in a non-linear relation between ϕ_c and i_c. Macro-cell current density at the point, i_{macro}, can then be determined from the following equation (note that the sign convention for the current density is positive for i_a and negative for i_c),

$$i_{macro} = i_a - i_c \quad (8)$$

According to Ohm's law, the normal gradient of potential at the steel surface is proportional to the macro-cell current, that is,

$$\frac{1}{r}\frac{\partial\phi}{\partial n} = i_{macro} \quad (9)$$

where r is the electrical resistance of concrete (Ωm) and n is the direction normal to the steel surface.

3. Corrosion analysis

If the electrical resistance of concrete is assumed to be isotropic, the distribution of electric potential is governed by Laplace's equation [11].

$$\nabla^2\phi = 0 \quad (10)$$

where ϕ is the electric potential (V) and ∇^2 is the Laplacian operator. To obtain the potential distribution in concrete, the solution of Eq. (10) subjected to the boundary condition of Eq. (9) should be found. Since both sides of Eq. (9) are dependent on the distribution of potential, this problem cannot be solved explicitly. Additionally, an essential boundary condition should be imposed manually since a unique solution cannot be obtained solely from the natural boundary conditions. The solution strategy developed in this study is as follows:

① Select a pivot point and assign an essential boundary condition with the pivot potential value (=ϕ_{pivot}).
② Assume initial distribution of potential.
③ Calculate the macro-cell currents at the boundary using Eqs. (6)–(8).
④ Construct the natural boundary conditions using Eq. (9).
⑤ Calculate the distribution of potential from the boundary conditions.
⑥ Repeat steps ③ to ⑤ until the norm in convergence test, $\|n\|$, is lower than the allowable limit value, $\|n\|_{allow}$.

$$\|n\| = \sqrt{\frac{\sum_{i=1}^{nn}[\{\phi_i\}^j - \{\phi_i\}^{j-1}]^2}{nn}} \leqslant \|n\|_{allow} \quad (11)$$

where $\{\phi_i\}^j$ is the potential value at the ith node after jth iteration and nn is the number of nodes.

⑦ Adjust the pivot potential value and repeat steps ① to ⑥ until the absolute difference between the corrosion current obtained from the normal gradient of potential and the macro-cell current obtained from the potential at the pivot point is lower than the allowable value, α_{allow}.

$$\left|\frac{1}{r}\frac{\partial\phi}{\partial n} - i_{macro}\right|_{\text{at the pivot}} \leqslant \alpha_{allow} \quad (12)$$

From the anodic current density, corrosion depth can be calculated as the following equation [1].

$$d_{corr} = \int 1.15\times10^4 i_a \mathrm{d}t \quad (13)$$

where d_{corr} is the corrosion depth (mm) and t is the time (year).

After the corrosion analysis, the following boundary condition is applied to the oxygen analysis to consider

the consumption of oxygen due to the cathodic reaction [11],

$$\frac{\partial C_{O_2}}{\partial n} = \frac{i_c}{4FD_{O_2}} \tag{14}$$

where C_{O_2} is the concentration of oxygen and D_{O_2} is the diffusion coefficient of oxygen.

The detailed procedure for the corrosion analysis including the diffusion analyses of chloride ion and oxygen is illustrated in Fig. 2.

4. Analysis results

4.1. General

Fig. 3 represents the finite element mesh constructed for the corrosion analysis; the diameter of steel is 20 mm, the depth of concrete cover is 50 mm, and the horizontal spacing of steel is 200 mm. Only the top surface of concrete is exposed to chloride ion and oxygen. Material properties used for the analysis are summarized in Table 1. The diffusion coefficient of chloride ion (D_{Cl}) and oxygen, as well as the electrical resistance of concrete, are selected as essential material properties for the parametric study since these properties varies considerably according to the quality of concrete and have strong influence on the corrosion behavior. On the other hand, the environmental parameters have little influence on the corrosion and the polarization properties are almost constant regardless of the quality of concrete. The ranges of these properties are determined from the representative values for concrete of a practical strength range [19–21].

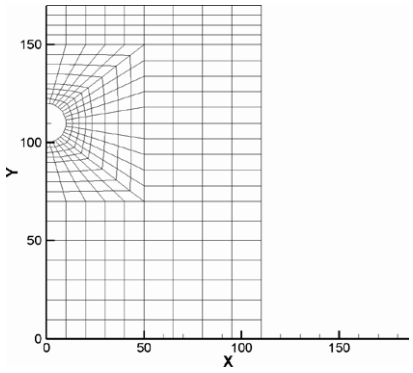

Fig. 3. Finite element mesh.

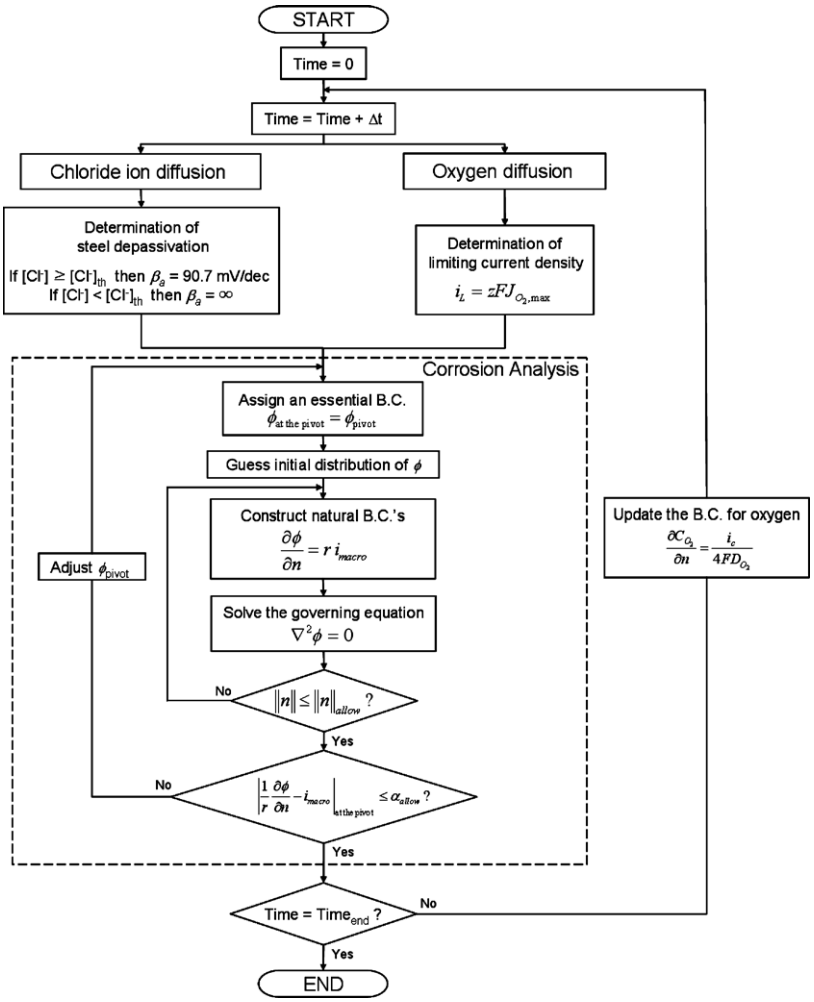

Fig. 2. Flowchart of the corrosion analysis.

Table 1
Values of material properties used for the corrosion analysis

Properties	Value
Diffusion coefficient of oxygen ($\times 10^{-9}$ m^2/s)[a]	2, 5, 10, 20
Diffusion coefficient of chloride ion ($\times 10^{-12}$ m^2/s)[a]	1, 2, 5, 10
Electrical resistance of concrete (Ohm m)[a]	50, 150, 500, 1000
External oxygen concentration (kg/m^3 solution)	0.0085
Initial oxygen concentration (kg/m^3 solution)	0.005
External concentration of chloride ion (% wt concrete)	1.0
Threshold concentration of chloride ion (% wt concrete)	0.05
Cathodic exchange current density (A/cm^2)	6×10^{-10}
Anodic exchange current density (A/cm^2)	2.75×10^{-8}
Cathodic equilibrium potential (mV vs. SCE)	160
Anodic equilibrium potential (mV vs. SCE)	−690

[a] Underlined values are the standard values for the parametric study.

Fig. 4a and b show a typical distribution of chloride ions around the steel and the corresponding distribution of corrosion potential, respectively. From these figures, accumulation of chloride ions at the upper part of steel and the more negative value of corrosion potential in this chloride-ion rich area can be confirmed.

Fig. 4c shows the typical time history of averaged corrosion currents – total, macro-cell, micro-cell. Corroding time is defined as the time after the initial depassivation of steel. That is, corroding time starts from zero when the concentration of chloride ion at the topmost point of steel becomes larger than the threshold value. It is clear that the early stage of corrosion is controlled by macro-cell corrosion. As the depassivated region extends, however, the contribution of macro-cell corrosion diminishes and finally micro-cell corrosion prevails. These analysis results correspond well with Mohammed's experimental observations [22].

Fig. 4d illustrates typical profiles of corrosion depth (solid lines) and average corrosion depth (dashed lines) for various corroding times. Distance from the top surface of steel on the abscissa is defined as the circumferential distance between the top point of steel and a specific point on the steel surface. We can clearly see the localized nature of corrosion. The ratio of the maximum corrosion depth to the average corrosion depth, which will be referred to as R_{corr}, is greatest at the early stage and gradually decreases; R_{corr} is about 5.9 at 0.2 years and 2.2 at 2 years. R_{corr} values obtained from the analysis are quite lower than the values found from experimental observations ($\approx 4 \sim 8$) [23,24]. The limitation of the analysis target to the two-dimensional corrosion likely accounts for this underestimation. From these observations, it can be concluded that a uniform shape of corrosion, as usually adapted in existing studies on the estimation of cracking time, is an over-simplification of the real corrosion shape, even for the two-dimensional corrosion.

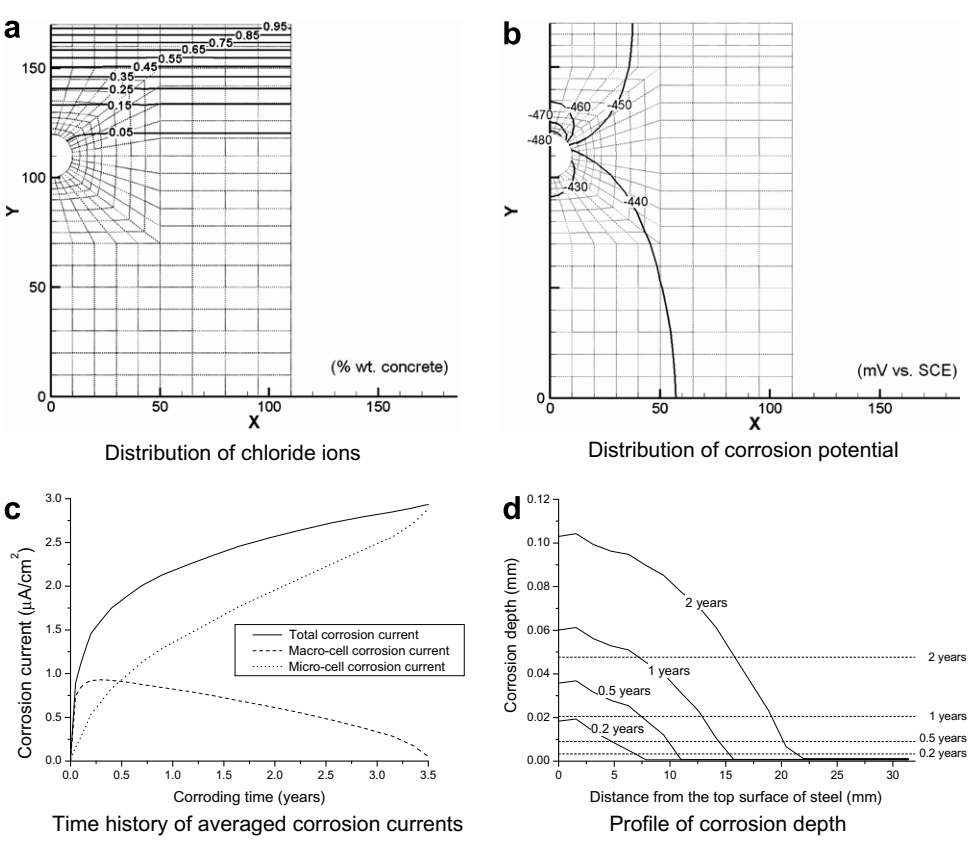

Fig. 4. Typical analysis results.

4.2. Parametric study

It is evident that the most decisive factors affecting the cracking time of concrete cover are the average corrosion current and R_{corr}, which indicate the rate of corrosion and the intensity of corrosion localization, respectively. In this section, the influence of material properties – diffusion coefficient of chloride ion and oxygen, and electrical resistance of concrete – on those parameters is numerically investigated. Plotting ranges of corroding time are limited to 3.5 years, which is a sufficiently long time for the concrete cover of most RC structures to be cracked, for all cases.

As shown in Fig. 5a, the diffusion coefficient of chloride ion is mainly related to the increase rate of corrosion current. As D_{Cl} increases, the depassivated region grows faster. Consequently, the time for the corrosion current to reach the maximum corrosion current, which is relevant

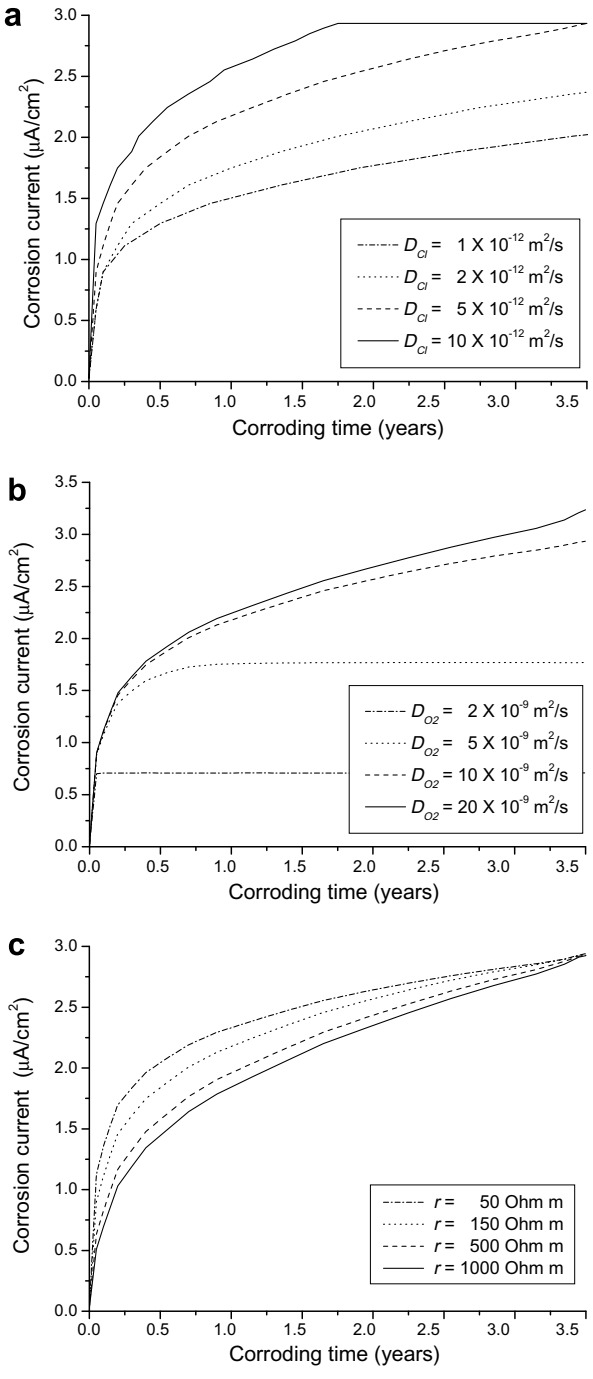

Fig. 5. Influence of material parameters on the average corrosion current (a) Influence of the diffusion coefficient of chloride ion; (b) Influence of the diffusion coefficient of oxygen and (c) Influence of the electrical resistance of concrete.

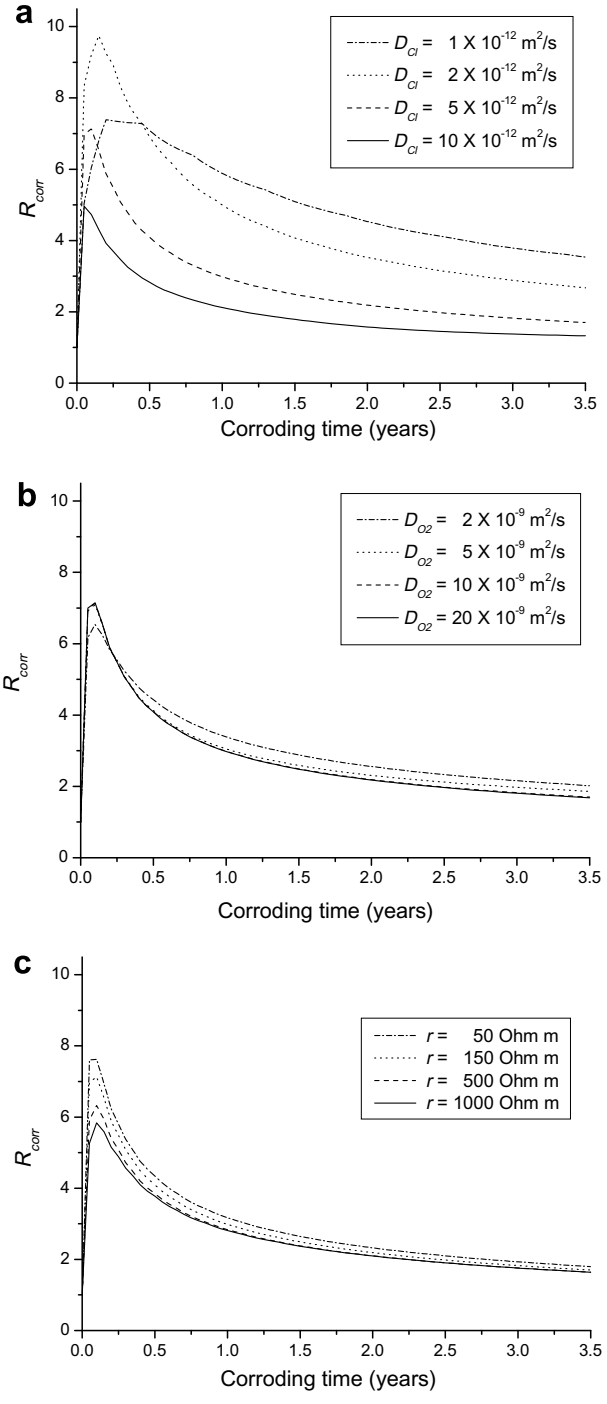

Fig. 6. Influence of material parameters on R_{corr} (a) Influence of the diffusion coefficient of chloride ion; (b) Influence of the diffusion coefficient of oxygen and (c) Influence of the electrical resistance of concrete.

to the polarization properties, becomes shorter. We can clearly see in Fig. 5b that when D_{O_2} is low, the maximum corrosion current is significantly restricted by the limiting corrosion current of the cathode, which is roughly proportional to D_{O_2}. This restriction, however, is negligible if D_{O_2} is higher than a specific value. In this situation, other properties of the polarization – Tafel slopes, equilibrium potentials, exchanging current densities – become crucial for the determination of maximum corrosion current. In Fig. 5c, the resistance of concrete appears to affect the increase rate of corrosion current. This is obvious since a greater portion of the steel surface becomes available to serve as a cathode, which contributes to an increase in the corrosion rate at the anodes via macro-cell corrosion, as the resistance of concrete decreases.

As shown in Fig. 6a, D_{Cl} has a strong influence on the corrosion localization. As D_{Cl} decreases, the period during which the depassivated regions are separated from the passive region is extended. As a result, the shape of corrosion depth becomes more irregular. The abnormally low value of R_{corr} for the case of $D = 10^{-12}\,m^2/s$ at the early stage results from the prolonged duration of the initiation stage, which leads to increased depth of uniform corrosion generated during the passive state of steel. The influences of D_{O_2} and r on the corrosion localization are not as apparent in Fig. 6b and c. However, if the longitudinal variation of corrosion state were considered, the influence of r would be remarkable because of the additional contribution of large scale macro-cell corrosion.

5. Discussion

Numerous research trials have been conducted to identify the critical corrosion depth that leads to corrosion induced cracking and subsequently the end of service life [1–8,24]. For example, Torres-Acosta et al. concluded statistically that the maximum crack width at the surface of concrete becomes 0.1 mm when the average corrosion depth reaches about 0.9 % of the steel radius [24]. If we define this as the end of service life, the duration of the propagation stage can be roughly estimated from the average corrosion current. However, there remain uncertainties regarding the influence of localized corrosion shape and, unfortunately, this influence has yet to be clearly quantified. According to Jang's numerical study, highly localized corrosion ($R_{corr} = 8$) shortens the duration of propagation stage to 60% of that based on the uniform corrosion [25]. For the precise assessment of the service life of RC structures, accurate quantification of the shape of localized corrosion is urgently needed. Owing to the random nature of corrosion, however, the determination of a realistic, representative shape of localized corrosion from experiment is almost impossible. In the authors' opinion, a numerical analysis can be a reasonable alternative to address this problem. We expect that subsequent research work that includes the influence of longitudinal variation could reproduce the real nature of corrosion more precisely.

Another advantage of numerical study is that the results can be directly applied to the mechanical analysis of crack propagation. After developing a unified program that can consider crack propagation as well as corrosion, we will be able to estimate the service life of RC structures explicitly from the material properties, including the fracture characteristics and the structural dimensions, instead of predicting it approximately from empirical models.

6. Conclusions

In this study, the localize shape of steel corrosion was numerically estimated considering the variation of chloride ions around the steel. Based on the analysis results, the following conclusions have been derived.

1. The calculated corrosion shape shows significant localization. The maximum corrosion depth remains about $1.3 \sim 3.5$ times deeper than the average corrosion depth after 3.5 years of active corrosion. Most of the corrosion damage occurs at the upper part of the steel, where the concentration of chloride ions is higher. For the accurate estimation of the service life of RC structures, the influence of corrosion localization should be considered.
2. According to the parametric study, the parameter most responsible for corrosion localization is the diffusion coefficient of chloride ion, which determines the expansion rate of the depassivated region on the steel surface.

Acknowledgements

The authors would like to thank the Infra-Structures Assessment Research Center (ISARC) funded by the Korea Ministry of Construction and Transportation (MOCT) for financial support.

References

[1] Andrade C, Alonso C. Cover cracking as a function of bar corrosion: part I – experimental test. Mater Struct 1993;26(8):453–64.
[2] Molina FJ, Alonso C, Andrade C. Cover cracking as a function of rebar corrosion: part 2 – numerical model. Mater Struct 1993;26(9):532–48.
[3] Bhargava K, Ghosh AK, Mori Y, Ramanujam S. Modeling of time to corrosion induced cover cracking in reinforced concrete structures. Cement Concrete Res 2005;35(11):2203–18.
[4] Dagher HJ, Kulendran S. Finite element modeling of corrosion damage in concrete structures. ACI Struct J 1992;89(6):699–708.
[5] Li CQ, Melchers RE, Zheng JJ. Analytical model for corrosion induced crack width in reinforced concrete structures. ACI Struct J 2006;103(4):479–87.
[6] Ohtsu M, Yosimura S. Analysis of crack propagation and crack initiation due to corrosion of reinforcement. Constr Build Mater 1997;11(7-8):437–42.
[7] Hansen EJ, Saouma VE. Numerical simulation of reinforced concrete deterioration – part II: steel corrosion and concrete cracking. ACI Mater J 1999;96(3):331–9.
[8] Liu Y, Weyers RE. Modeling the time to corrosion cracking in chloride contaminated reinforced concrete structures. ACI Mater J 1998;95(6):675–81.

[9] Nam J, Hartt WH, Kim K. The effects of cement alkalinity upon the pore water alkalinity and the chloride threshold level of reinforcing steel in concrete. J Korea Concrete Inst 2004;16(4):549–55.
[10] Kranc SC, Sagüés AA. Detailed modeling of corrosion macrocells on steel reinforcing in concrete. Corr Sci 2001;43(7):1355–72.
[11] Isgor OB, Razaqpur AG. Modeling steel corrosion in concrete structures. Mater Struct 2006;39(3):291–302.
[12] Maruya T, Hsu K, Takeda H, Tangtermsirikul S. Numerical modeling of steel corrosion in concrete structures due to chloride ion, oxygen and water movement. J Adv Concrete Technol 2003;1(2):147–60.
[13] Raupach M, Warkus J, Yamaguchi T. Numerical modeling of reinforcement corrosion. Proceedings of the ESCS 2006, Espoo Finland; p. 282–88.
[14] Kranc SC, Sagüés AA. Computation of reinforcing steel corrosion distribution in concrete marine bridge substructures. Corr Sci 1994;50(1):50–61.
[15] Gulikers J. Numerical modeling of reinforcement corrosion in concrete. In: Corros Reinforced Concrete Struct. Woodhead Publishing Limited, CRC Press; 2005. p. 71–90.
[16] Oh BH, Jang BS. Chloride diffusion analysis of concrete structures considering effects of reinforcements. ACI Mater J 2003;100(2):143–9.
[17] Hansen EJ, Saouma VE. Numerical simulation of reinforced concrete deterioration – part I: chloride diffusion. ACI Mater J 1999;96(2): 173–80.
[18] Uhlig HH, Revie RW. Corrosion and corrosion control. John Wiley and Sons; 1985. p. 35–59.
[19] Papadakis VG, Vayenas CG, Fardis MN. Physical and chemical characteristics affecting the durability of concrete. ACI Mater J 1991;88(2):186–96.
[20] Oh BH, Jang SY. Prediction of diffusivity of concrete based on simple analytic equations. Cement Concrete Res 2004;34(3):463–80.
[21] Saleem M, Shameem M, Hussain SE, Maslehuddin M. Effect of moisture, chloride and sulphate contamination on the electrical resistivity of Portland cement concrete. Constr Build Mater 1996;10(3):209–14.
[22] Mohammed TU, Hamada H. Corrosion of steel bars in cracked concrete: very beginning to the early age of exposure. ACI SP 235, 2006. p. 103–23.
[23] González JA, Andrade C, Alonso C, Feliu S. Comparison of rates of general corrosion and maximum pitting penetration on concrete embedded steel reinforcement. Cement Concrete Res 1995;25(2):257–64.
[24] Torres-Acosta AA, Madrid MM. Residual life of corroding reinforced concrete structures in marine environment. J Mater Civil Eng 2003;15(4):344–53.
[25] Jang BS. Life time estimation method of reinforced concrete structures considering the effects of reinforcements on the chloride diffusion and the non-uniform corrosion distribution. Ph.D. Thesis, Department of Civil Engineering, Seoul National University, 2001.